HHS Public Access

Author manuscript

Acta Biomater. Author manuscript; available in PMC 2018 October 15.

Published in final edited form as:

Acta Biomater. 2017 October 15; 62: 116–127. doi:10.1016/j.actbio.2017.08.009.

Elastin-PLGA Hybrid Electrospun Nanofiber Scaffolds for Salivary Epithelial Cell Self-Organization and Polarization

Zahraa I. Foraida[1], **Tim Kamaldinov**[1], **Deirdre A. Nelson**[2], **Melinda Larsen**[2,a], and **James Castracane**[1,a]

[1]Colleges of Nanoscale Science and Engineering, SUNY Polytechnic Institute

[2]Department of Biological Sciences, University at Albany, State University of New York

Abstract

Development of electrospun nanofibers that mimic the structural, mechanical and biochemical properties of natural extracellular matrices (ECMs) is a promising approach for tissue regeneration. Electrospun fibers of synthetic polymers partially mimic the topography of the ECM, however, their high stiffness, poor hydrophilicity and lack of *in vivo*-like biochemical cues is not optimal for epithelial cell self-organization and function. In search of a biomimetic scaffold for salivary gland tissue regeneration, we investigated the potential of elastin, an ECM protein, to generate elastin hybrid nanofibers that have favorable physical and biochemical properties for regeneration of the salivary glands. Elastin was introduced to our previously developed poly-lactic-co-glycolic acid (PLGA) nanofiber scaffolds by two methods, blend electrospinning (EP-blend) and covalent conjugation (EP-covalent). Both methods for elastin incorporation into the nanofibers improved the wettability of the scaffolds while only blend electrospinning of elastin-PLGA nanofibers and not surface conjugation of elastin to PLGA fibers, conferred increased elasticity to the nanofibers measured by Young's modulus. After two days, only the blend electrospun nanofiber scaffolds facilitated epithelial cell self-organization into cell clusters, assessed with nuclear area and nearest neighbor distance measurements, leading to the apicobasal polarization of salivary gland epithelial cells after six days, which is vital for cell function. This study suggests that elastin electrospun nanofiber scaffolds have potential application in regenerative therapies for salivary glands and other epithelial organs.

Graphical Abstract

[a]Corresponding authors: Melinda Larsen, Ph.D., Department of Biological Sciences, University at Albany, State University of New York, 1400 Washington Ave., Albany, NY 12203, mlarsen@albany.edu; James Castracane, Ph.D., Colleges of Nanoscale Science and Engineering, SUNY Polytechnic Institute, 257 Fuller Rd., Albany, NY 12203, Jcastracane@sunypoly.edu.

Disclosures

None.

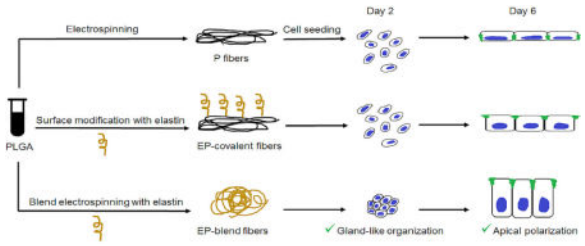

Keywords

Elastin; nanofibers; salivary gland; tissue regeneration; epithelial polarity; cell organization

1. Introduction

Loss of saliva termed salivary hypofunction due to salivary gland damage from head and neck radiation therapy, the autoimmune disease Sjögren's syndrome, and other causes significantly affects the quality of patients' lives by negatively impacting speaking, swallowing, digestion and oral health. Current treatments provide only short term symptomatic relief or carry a plethora of side effects, [1–3], creating interest in bioengineered salivary glands for restoration of salivary function. Salivary glands are composed of a hollow branched network of ducts terminating in acini that produce saliva. The ductal and acinar cells comprising the luminal surface are polarized tightly-organized epithelial cells [4]. Tight junction proteins, such as occludin and zonula occludin-1 (ZO-1), localize preferentially towards the apical (top) surface and play an important role in maintaining apicobasal polarization. Correct polarization and tight-junction clustered cell organization are vital for normal epithelial barrier function and regulation of proliferation [5–7], and disruption of polarity is one of the first steps during salivary gland tumorigenesis [8–10]. Promotion of apicobasal polarization of salivary epithelial cells is thus an important requirement for bioengineered scaffolds to restore salivary function.

One of the promising biomaterial-based approaches to regenerate the salivary epithelium is by mimicking the chemical, topographical, and the mechanical properties of the basement membranes and extracellular matrix (ECM). The basement membranes, a specialized form of the extracellular matrix (ECM), and the ECM are in close proximity to the polarized epithelial cells. They are fibrous sheets of proteins that provide mechanical support and chemical signals for tissue morphogenesis, among other functions. The topography, mechanical properties, and chemical composition of the basement membranes and ECM can activate cell signaling pathways to influence cellular behavior, including a myriad of effects on cellular shape, adhesion, migration, proliferation and differentiation [11].

Mechanically, the compliance of the extracellular environment of cells impacts their ability to undergo both developmental and regenerative processes [19]. To understand the contribution of compliance to morphogenesis and differentiation of developing submandibular salivary glands, we previously engineered artificial environments of differing compliance [20–22]. Embryonic salivary gland organ explants underwent morphogenesis and differentiation most similar to the *in vivo* processes in a compliant environment. To

facilitate tissue engineering-based regenerative medicine, we previously engineered PLGA nanofiber scaffolds to mirror the topography [23–24] and some chemical properties [14] of the basement membrane. However, the PLGA nanofiber scaffolds are orders of magnitude less compliant than adult salivary glands [20–21], suggesting the need for more compliant nanofiber scaffolds.

Chemically, the main components of the basement membrane are collagen IV, elastin, the laminin-nidogen complex and perlecan [11–12]. Several research groups have incorporated basement membrane components into scaffolds developed to biochemically mimic the native ECM of the glands and promising results were obtained [14–18]. Laminin [14–15], perlecan peptide [16–17], fibronectin and collagen [18] were utilized for salivary cell regeneration [14–18]. However, the potential utility for elastin in scaffolds to advance salivary gland tissue engineering strategies has not been examined.

Elastin serves both structural and biochemical roles. It is responsible for tissue compliance and it contains peptide sequences identified to induce differentiation, migration and proliferation [25–32]. It is responsible for the elasticity of the skin [29], lungs [27] and blood vessels [26]. In addition, several biochemical roles were attributed to elastin peptides including keratinocyte differentiation and chemotaxis [33], cell adhesion [28] and mesenchymal stem cell differentiation [34]. *In vivo*, elastin is abundant in the duct system of the rat submandibular salivary glands extending from the ECM into the basement membrane of the salivary epithelial cells [35–36]. It is thought to provide the needed elasticity for the gland to withstand the repeated tension-relaxation cycles associated with saliva flow and head and neck movement. Therefore, it has a role in defining the salivary cell shape and cell-cell distance [35]. Additionally, several research groups have introduced elastin for tissue engineering applications, where it has demonstrated promising results for the regeneration of various tissues. Elastin promoted skin regeneration [37–39], *in vivo*-like organization of hepatocytes [40] and elasticity for blood vessel engineering [41–52].

In this study, we build upon our previous work by incorporating elastin into PLGA nanofiber scaffolds [53, 14, 23–24]. We hypothesize that elastin will 1) improve the compliance and 2) hydrophilicity of the scaffolds and 3) provide *in vivo*-like biochemical cues for cell organization. To distinguish between the elastic properties of the nanofibers and the chemical signals imparted by elastin, elastin was introduced to PLGA nanofibers by two methods: blend electrospinning and covalent conjugation. The contribution of elastin to the physical and mechanical properties of the PLGA nanofiber scaffolds in both configurations was characterized. Additionally, both types of elastin nanofiber scaffolds were assessed for their ability to support the proliferation, apical polarization, and epithelial morphology of the immortalized submandibular salivary epithelial cell line (SIMS).

2. Materials and methods

2.1. Synthesis of the nanofiber scaffolds

Soluble (hydrolyzed) elastin (ES12) was purchased from Elastin Products (Owensville, MO), poly(D-lactide-co-glycolide) (PLGA), (B6006-1) with a molecular weight of 95000 Da and a lactic to glycolic acid ratio of 85:15 was purchased from Birmingham Polymers

(Pelham, AL), and the solvent used to dissolve both components, hexafluoroisopropanol (HFIP) (922661), was purchased from Sigma Aldrich (St. Louis, MO). For covalent conjugation of elastin on the surface of PLGA fibers, 1-ethyl-3-(3-dimethylaminopropyl) carbodiimide (EDC) (39391), N-hydroxysuccinimide (NHS) (130672), and 2-(N-morpholino) ethanesulfonic acid (MES) solution (M1317) were from Sigma Aldrich. Sulphorhodamine B (SRB) was used to label the nanofibers for confocal imaging and was purchased from (Life Technologies, Grand Island NY). The electrospinning set up consists of a syringe pump (model # NE 300) that was purchased from New Era Pump Systems (Farmingdale, NY) and the high voltage supply (model # ES100) was purchased from Gamma High Voltage Research (Ormond beach, FL).

2.1.1 Preparation of Elastin-PLGA nanofibers by blend electrospinning (EP-blend)—Equal weights of 8% w/w soluble elastin in HFIP (hydrolyzed elastin from bovine neck ligament) and of 8% w/w PLGA in HFIP were mixed together to yield a solution containing 4% elastin and 4% PLGA (w/w). Sodium chloride (1% w/w) was added to the solution before electrospinning to minimize beading. In addition, 2.5 μM Sulphorhodamine B (SRB) was added to the solution to label the fiber mats for confocal microscopy imaging. The solution was pumped through a 3-mL syringe, which was connected to an automated micro-syringe pump through polytetrafluoroethylene (PTFE) tubing to a (25 G) needle. The needle tip and the aluminum foil-coated collector ground were both connected to a high voltage source (14 kV). The voltage was applied to the needle tip and the collector ground while pumping the blend polymer solution at a rate of 6 μL/min and a distance between the needle tip and the collector ground of 15 cm. The nanofibers were formed and collected on the collector ground. For cell culture experiments, the fibers were electrospun on 13 mm glass coverslips sitting on the foil surface. The glass coverslips were covered with an adhesive layer of 3% (w/w) PLGA in HFIP solution that polymerized for 45 minutes before electrospinning to prevent the delamination of the fibers when soaked for extended periods of time.

2.1.2 Preparation of PLGA nanofibers (P)—PLGA nanofibers were prepared by electrospinning of 8% (w/w) PLGA in HFIP, as described previously [53, 14, 23–24], to generate nanofibers having a mean diameter of ~ 250 nm. Sodium chloride (1% w/w) was added to the solution before electrospinning to minimize beading and Sulphorhodamine B (SRB) (2.5 μM) was added to the solution to label the fiber mats for confocal microscopy.

EP-blend nanofibers were electrospun for 45 minutes at a rate of 6 μL/min, and P nanofibers were electrospun for 90 minutes at a rate of 3 μL/min to equalize the thickness of the mats for all characterization tests and cell culture experiments.

2.1.3 Covalent conjugation of elastin to PLGA nanofibers (EP-covalent)—The (EP-covalent) nanofibers were synthesized by covalent conjugation of elastin (hydrolyzed elastin from bovine neck ligament) on the surface of PLGA (P) nanofibers using EDC-NHS chemistry, as previously described in [14, 54] for conjugation of different proteins and peptides to polymeric nanofibers. Briefly, activation of the carboxylic acid groups of PLGA within electrospun PLGA nanofiber scaffolds was carried out by plasma treatment for 5 minutes using Harrick plasma PDC-32G Plasma Cleaner (Boston Industries, Walpole, MA)

followed by soaking in a solution of 4 mM 1-ethyl-3-(3-dimethylaminopropyl) carbodiimide (EDC), 100 mM N-hydroxysuccinimide (NHS), 0.1 M 2-(N-morpholino) ethanesulfonic acid (MES) solution, pH = 5 for 1 h at room temperature. Scaffolds were then washed with 1× PBS before incubating with a solution of elastin in 1× PBS (5 mg elastin/1mL PBS/sample) overnight at 4°C and stored in 1× PBS at 4°C.

2.2. Characterization of the scaffolds

2.2.1. XPS—X-ray photoelectron spectroscopy (XPS) was used to confirm the inclusion of both PLGA and elastin in the scaffolds. XPS spectra were recorded using a Thermo Scientific Theta Probe™ system with a monochromatic Al K_α (1486.6 eV) x-rays of 400 μm spot size, energy step size of 1 eV, and pass energy of 100 eV.

2.2.2. FTIR—Fourier Transform Infrared spectroscopy (FTIR) was used to confirm the successful inclusion of elastin and PLGA in the scaffolds by the appearance of their specific absorbance peaks. FTIR spectra were recorded using a Bruker Tensor 27 FTIR spectrometer (Bruker Corporation, Billerica, MA, USA) in Attenuated Total Reflectance module (ATR) with a resolution of 4 cm^{-1} in the range between 400–4000 cm^{-1}, and only the region of interest is shown. Bio-Rad software was used for spectral data analysis and plotting.

2.2.3. Determination of elastin content of scaffolds—To determine the total elastin content in each of the scaffold types, UV absorbance spectroscopy was used. Briefly, known weights of EP-blend and EP-covalent scaffolds were completely dissolved in 0.1 mL HFIP. After the nanofibers were completely dissolved, the volume was completed to 1 mL with 1X PBS. The absorbance of 0.1 mL of the supernatant was measured at 280 nm using a microplate reader (TECAN, Switzerland). Using a standard curve of elastin protein ($y = 5.9718x + 0.042$, $R^2 = 0.9983$), the elastin concentration and the total content were calculated. Four independent measurements were taken for each scaffold type.

2.2.4. SEM—Scanning electron microscopy (SEM) imaging of the scaffolds was carried out using a Zeiss 1550 field emission scanning electron microscope (Leo Electron Microscopy Ltd., Cambridge, UK; Carl Zeiss, Jena, Germany), as described previously [24]. Briefly, the scaffolds were mounted on 1 cm^2 stubs and coated with approximately 5 nm of gold-palladium to minimize sample charging. Images were captured using an in-lens detector, 1–5 kV acceleration voltage and a working distance of 2–6 mm. The microscope annotation software was used to apply scale bars, and ImageJ software was used to measure the fiber diameters from calibrated images. At least 4 scaffolds of each type were imaged and 200 nanofibers analyzed for average fiber diameter measurements.

2.2.5. AFM—PeakForce Quantitative Nanomechanical Mapping of nanofibrous scaffolds was performed on a Bruker BioScope Catalyst (Bruker) atomic force microscope (AFM) mounted on a Leica SP5 confocal microscope base (Leica Microsystems). Mechanical measurements were performed with silicon nitride cantilevers of nominal spring constant 5.4 N/m that were functionalized with 12 um borosilicate glass particles (Novascan). The thermal tune method was used to determine the actual spring constant of the cantilever, and the radius of the probe was calibrated to match the modulus of the reference standard

(polydimethylsiloxane, 3.5 MPa, Bruker). Peak Force Setpoint was adjusted to achieve the same indentation on unknown samples as on the reference standard. Indentations of 200–500 nm were used as determined by either analyzing the force curves for softer samples (Bruker Nanoscope Analysis v1.5) or the deformation maps for stiffer samples. The electrospun fibers for AFM measurements were prepared as described in section 2.1 (synthesis of the nanofiber scaffolds) without addition of SRB dye. All measurements were performed in air on dry scaffolds. A total of 32 measurements were recorded for elastin-PLGA-blend and PLGA samples, and a total of 8 measurements were recorded for elastin-PLGA-covalent and PLGA-EDC samples.

2.2.6. Contact angle measurements—The wettability of the nanofibrous scaffolds and glass substrates was measured using a CAM-PLUS contact angle meter (Cheminstruments, Fairfield, OH). A deionized water drop of 10 μL was placed on the scaffold from an automated syringe and the reading of the contact angle was recorded. Four samples of each scaffold type were measured and their mean was calculated.

2.3. Cell culture

Before cell culture experiments, nanofiber scaffolds and glass substrates were UV sterilized for 1 hour and then soaked in 1% v/v Penicillin/Streptomycin in 1× PBS overnight at 37°C to remove any remaining solvents and to eradicate bacterial contamination. SIMS cells, an immortalized mouse ductal submandibular epithelial cell line, [55] were cultured as previously reported [14, 23–24]. The cells were incubated to attach and grow on the scaffolds using 24 well plates in a humidified incubator at 37°C and 5% CO_2.

2.4. Cell proliferation assay

A cell proliferation assay was performed similar to our previous report [14]. SIMS cells seeded at 50,000 cells/ml were allowed to attach to scaffolds and grown for 4, 24, 48 and 72 hours. At the specified time interval, the scaffolds were transferred to a new 24-well plate to avoid counting cells growing on the plate rather than the scaffolds, washed with 1× PBS and collected using 0.25% trypsin-EDTA (Gibco). Cells were pelleted, re-suspended in 50 μL of culture media to which an equal volume 0.4% trypan blue solution (1450021, Bio Rad Hercules, California) was added, incubated for 5 minutes, and viable cells were counted using an automated cell counter (BioRad TC20 automated cell counter). The experiment was repeated three times.

2.5. Immunocytochemistry and confocal imaging

SIMS cells cultured on scaffolds were fixed using 1 mL of fresh 2% paraformaldehyde solution, 5% sucrose in 1× PBS for 20 minutes. Samples were washed with 0.5% Tween 20 in 1× PBS (PBS-T), permeabilized for 15 minutes in 0.1% Triton X-100, and blocked with 20% donkey serum in PBS-T for 2 hours. Primary antibodies to occludin (33-1500, Life Technologies) and ZO-1 (40-2200, Life Technologies) diluted 1:100 in a solution of 3% BSA in PBS-T were allowed to rock overnight at 4°C and washed four times with PBS-T. Secondary antibodies diluted 1:250 in 3% BSA in PBS-T were incubated for 2 hours at room temperature. Secondary antibody solutions included the nuclear stain 4′,6-diamidino-2-phenylindole (DAPI) (D1306) and Alexafluor-488 phalloidin at a dilution of

(1:50) to stain filamentous actin (F-actin). Samples were washed 4 times with PBS-T and mounted using 1% p-phenylenediamine (PPD) (P6001, Sigma Aldrich) antifade solution in Fluor-gel mounting media (17985-10EMS, Hatfield, PA), on thin plastic coverslips and air dried overnight. The dried samples were sealed using clear nail polish and stored at −20 °C until imaging. The images as well as the Z-stacks of cells on different substrates were acquired using a Leica SP5 laser scanning confocal microscope (Leica Microsystems, Mannheim, Germany).

2.6. Nuclear area and nearest neighbor distance measurements

Confocal images (63× magnification) of DAPI-stained nuclei were analyzed using ImageJ software to obtain the average nuclear area as an indicator of cell spreading and the nucleus-nucleus nearest neighbor distance (NND) as an indicator of how closely cells are associated. Image analysis for the nuclear area and for the nearest neighbor distance was performed as described previously [56]. Briefly, the scale bars of the images were inserted into the software using “set scale” function. The images were converted to 8-bit images then binarized using “make binary function” and they were segmented using the “watershed” function to eliminate any overlapping nuclei. The images were then treated with “analyze particle” function to obtain the nuclear area and to eliminate measuring any small pre-apoptotic nuclei, the minimal nuclear area was set to 25 μm^2. For the nearest neighbor distance measurements, the “NND” plugin was employed after the previous steps. At least 3 images from each scaffold type were used to extract the nuclear area and NND between all the cells in each image.

2.7. Measurements of monolayer heights and infiltration depth

The XZ projections from confocal microscopy Z-stacks at magnification of 63× were acquired for cells cultured on scaffolds. Using the annotation software in the LasAF program and ImageJ software, the average cell monolayer height was quantified as described previously [24]. Briefly, the distance from the base of the nucleus (DAPI stain) corresponding to the basal side, to the stain of F-actin corresponding to the apical side was measured. At least 3 samples of each type were measured with 10 measurements each. In addition, in order to assess the cell-scaffold integration of the different substrates, the cell infiltration depth was measured. Using the confocal Z-stacks and the XZ projections, the infiltrated cell height (blue for nucleus and green for actin) embedded within the fibers (red) was measured in relation to the total cell height. The percentage infiltration depth was calculated as follows:

$$\%\ Infiltration\ depth = \frac{Embedded\ cell\ hieght}{Total\ cell\ height} * 100$$

At least 3 samples of each scaffold were measured with 10 measurements each.

2.8. Statistical analysis

Single-factor analysis of variance (ANOVA) with Bonferroni post-test was used to compare the means of different groups within each experiment. Degree of statistical significant difference was indicated as follows: *$p < 0.05$, **$p < 0.01$, ***$p < 0.001$.

3. Results

3.1. Confirmation of elastin incorporation into the nanofiber scaffolds

3.1.1 XPS—To generate PLGA nanofibers containing elastin in an attempt to increase their compliance and biomimetic characteristics, we incorporated elastin by blend electrospinning. As a control, we also incorporated elastin by chemical conjugation using EDC/NHS chemistry on the surface of PLGA nanofibers. Since XPS is a useful analytical method for both qualitative and quantitative atomic analysis of materials; we used it to confirm the presence of elastin in both the elastin-containing scaffolds, as compared to PLGA nanofibers. Figure 1 shows the XPS spectra of elastin-PLGA nanofiber scaffolds prepared by blend electrospinning (EP-blend) and covalent conjugation (EP-covalent). The appearance of carbon 1s (C1s) and oxygen 1s (O1s) peaks is attributed to the backbone of both elastin and PLGA. Most importantly, the appearance of the nitrogen 1s (N1s) peak around 400 eV range indicates the presence of elastin in both EP-blend and EP-covalent nanofibers; this peak is absent in the XPS spectrum of PLGA fibers. The XPS spectra of PLGA nanofibers are the closest to the typical C1s [57] and O1s [58] peaks of organic compounds; they are seen at 286 and 533 eV respectively. For EP-blend scaffolds, the C1s and O1s peaks shifted slightly to 282 and 528 eV, respectively, with the appearance of N1s peak at 396 eV. This shift may be attributed to non-covalent interactions between elastin and PLGA. As a protein, elastin contains electron-rich atoms such as oxygen and nitrogen. These atoms carry partial negative charge, and therefore may undergo electrostatic interactions with PLGA atoms. This is sensed by the atoms as abundance of electrons and manifested as electrostatic shift to lower binding energy [59–60]. On the other hand, In EP-covalent scaffolds, C1s, O1s and N1s peaks appear shifted to higher binding energy, 304, 548, and 417 eV, respectively. This can be explained by the fact that the covalent bond formed by EDC chemistry to conjugate elastin to PLGA changed the polarity and decreased the electron density around the nuclei which results in chemical shift to higher binding energy. Similar peak shifts as a result of covalent conjugation was seen elsewhere [61]. Detailed studies of the effects of electrostatic and chemical interactions on the XPS spectra is well-described in the literature [59–60].

3.1.2 FTIR—Qualitative FTIR analysis of the nanofiber scaffolds was carried out to: 1) confirm successful incorporation of both PLGA and elastin into the scaffolds and 2) verify that elastin did not undergo significant structural changes during incorporation into the scaffolds by electrospinning or covalent conjugation as indicated by the appearance of all its major peaks. As a protein, the FTIR spectra of elastin are dominated by the vibrational modes of amide bonds. Therefore, the suppression of native peaks or the appearance of new peaks may indicate disruption to the polypeptide/protein chain during scaffold synthesis [62–63]. Figure 2 shows the FTIR spectra of the hybrid elastin-PLGA nanofiber scaffolds in comparison to PLGA (P) and elastin powder (E). EP-blend and EP-covalent scaffolds

showed almost identical FTIR spectra, with the appearance of very prominent elastin-specific peaks, as indicated by its similarity to the FTIR spectrum of elastin powder. The two elastin-containing scaffolds showed peaks around 1650 and 1540 cm^{-1}, and they are attributed to N-C=O stretching vibrations of the primary and secondary amides in elastin, respectively [63]. This indicates that neither blend electrospinning nor covalent conjugation affected the main functional groups in elastin. All the nanofiber scaffolds showed characteristic PLGA peaks. The peak around 1753 cm^{-1} is attributed to C=O stretching vibration of the polymer backbone and the peaks around 1184, 1130, 1090 and 1050 cm^{-1} are assigned to C-O-C stretching vibration [64]. Slight up and down shifts of the peaks are attributed to differences of the local environment of the bonds and possible interactions with neighboring atoms causing changes in bond polarity. FTIR analysis confirmed the presence of intact elastin peptides in both the blend electrospinning and chemically conjugated elastin-PLGA nanofiber scaffolds.

3.1.3. Elastin content in the scaffolds—To quantify the total elastin content in each of the scaffolds, UV absorbance spectroscopy was used. The total elastin concentration was found to be 0.5666 ± 0.036 and 0.5587 ± 0.041 mg elastin/1 mg nanofibers for EP-blend and EP-covalent scaffolds respectively.

The distribution of elastin within the scaffolds in each type can be deduced from the synthesis method. The synthesis method is blend electrospinning for EP-bend and post-electrospinning surface functionalization in EP-covalent nanofibers. Both techniques are well-established and described in in the literature [65–69]. Blend electrospinning, the synthesis method of EP-blend, produces uniform distribution of the components of the nanofibers [65–67], especially when they are miscible within the same solvent, as is the case in EP-blend. Therefore, elastin is evenly distributed throughout the bulk and on surface of the fibers. On the other hand, post-electrospinning surface functionalization of nanofibers, as in the case of EP-covalent nanofibers, produces accumulation of the functional moiety on the surface of the nanofibers only [68–69]. Therefore, in EP-covalent nanofibers, the body of the nanofiber mat is made of electrospun PLGA fibers. These nanofibers are then surface modified with elastin through covalent conjugation.

3.2. SEM characterization of the scaffolds

To characterize the diameter and morphology of the elastin-PLGA nanofiber scaffolds, scanning electron microscopy (SEM) was carried out. In order to account only for the mechanical and chemical effects of elastin and minimize any possible morphological effects of elastin, we chose the concentrations of PLGA and elastin to obtain a similar fiber diameter to our previous reports of 8% PLGA [14, 23–24, 53]. Therefore, we kept the total solid content constant at 8% w/w (4% elastin and 4% PLGA) for EP-blend fibers. This successfully resulted in close fiber diameters. Figure 3 shows the SEM images of elastin-PLGA fibers (blend) and PLGA fibers. The mean fiber diameter was measured from SEM images and calculated to be 308 ± 130 and 250 ± 90 nm for elastin-PLGA-blend and PLGA fibers, respectively. However, despite the constant polymer content, EP-blend showed more tilts and bends than PLGA fibers. EP-covalent nanofibers are prepared as PLGA nanofibers followed by covalent conjugation of elastin by means of EDC chemistry. As expected and

shown in Figure 3, the diameter of the fibers is the same as for P scaffolds, with apparent fiber crosslinking induced by EDC chemistry. Surface-conjugated elastin is too small to be distinguished at this magnification.

3.3. Effect of elastin nanofiber modification on the scaffold stiffness

Given that elastin, as the functional component of elastic fibers, is largely responsible for the elasticity of ECM within many organs, it is expected that adding elastin to PLGA nanofibers will confer elasticity. To test this hypothesis, the average Young's modulus of the nanofiber mats was measured, as shown in Figure 4A. Elastin as a blend electrospinning component of the nanofibers (EP-blend) significantly increased the compliance, or decreased the stiffness, of the scaffold when compared to PLGA nanofibers; Young's modulus ~ 0.59 ± 0.356 MPa for EP-blend as compared to 4.29 ± 1.789 MPa for P. On the other hand, elastin as a surface modification (EP-covalent) had the opposite effect where it caused a significant increase in the mean scaffold stiffness and heterogeneity of the mechanical properties; Young's modulus ~ 20.72 ± 5.978 MPa. This can likely be attributed to the fact that the process of covalently conjugating elastin on the surface of PLGA fibers with EDC chemistry is known to crosslink nanofibers, thus increase the bulk stiffness of the material [71–72]. To confirm, the Young's modulus of PLGA nanofibers treated with EDC chemistry without the addition of elastin was measured; Young's modulus ~ 20.4 ± 8.6 MPa. As shown in Figure 4A, no significant difference was observed between PLGA fibers treated with EDC chemistry (P-EDC) and PLGA fibers conjugated with elastin using EDC chemistry (EP-covalent). Thus, the increase in the scaffold stiffness of elastin-PLGA scaffold prepared by covalent conjugation (EP-covalent) can be attributed to EDC crosslinking effect rather than elastin. AFM measurements were performed in dry conditions, which is different from the cells' wet environment. While it is expected that the mechanical properties of elastin may change in wet conditions, we expect that the values of elastic modulus in wet conditions may be lower than in air for all types of electrospun scaffolds that we fabricated, as reported elsewhere [73–74]; however, the trend is expected to be conserved [73–74].

Several reports have listed Young's moduli for elastin *in vivo*, the values vary depending on the tissue and the degree of crosslinking. For example, the elastic modulus values of elastin in bovine neck ligaments are ~ 1.1 MPa [75], porcine carotid atrial vessels ~ 0.45 MPa, and porcine aorta ~ 0.81 Mpa [76]. As for the electrospun fibers containing elastin, their elastic modulus values vary: ~ 0.33 MPa for crosslinked α-elastin [77] and 0.77 MPa for electrospun blend of PLGA, gelatin and elastin [44]. While the exact stiffness value of the salivary gland ECM was not reported before, the adult salivary glands' Young's moduli are in the 1–4 kPa range [21]. Therefore, PLGA nanofibers and similar materials are stiffer than the *in vivo* tissue. Therefore, incorporation of elastin into the nanofibers themselves by blend electrospinning (EP-blend) thus decreased the Young's modulus, meaning that the EP-blend nanofibers are more similar to the compliance of the natural tissue *in vivo* than either the PLGA nanofibers or the EP-covalent nanofibers [21], which should promote cellular self-organization [78].

3.4. Effect of elastin nanofiber modification on the wettability of the nanofiber scaffolds

Scaffold wettability is an important factor affecting the cell behavior, and hydrophilic surfaces have been found to be generally favorable for cell attachment [79–80]. To assess the effect of elastin functionalization on the wettability of the PLGA nanofiber scaffold, the water contact angle of the two elastin-containing scaffolds as compared to PLGA nanofibers and glass was measured, as shown in Figure 4B. The addition of elastin significantly increased the wettability of the nanofiber scaffolds whether it was introduced to the fiber mat by blend electrospinning or to the surface by covalent conjugation. The contact angle was significantly reduced from 110 ± 4.56° for PLGA to 42.17 ± 2.4° and 25 ± 5.25° for EP-blend and EP-covalent, respectively. The improvement of wettability upon the introduction of elastin agrees with previous reports showing a contact angle value of elastin (cast film) ~ 47° and when introduced to polytetrafluoroethylene (ePTFE) to make vascular grafts, it has a contact angle of 43° [81]. Also, human elastin-like polypeptides were reported to confer wettability to surfaces (contact angle ~ 24°) [82]. The wettability of the scaffolds increased most significantly following chemical conjugation of elastin onto the surface (EP-covalent), suggesting accumulation of more elastin on the scaffold surface as expected from the synthesis method (post-electrospinning surface modification).

3.5. Effect of elastin nanofiber modification on SIMS cell proliferation

Biochemically, elastin peptides were reported to modulate the proliferation of some cell types in different manners. For example, they suppressed the proliferation of keratinocytes [33] while they promoted the proliferation of smooth muscle cells [83] and fibroblasts [84–85]. In addition, polarization of epithelial cells is usually inversely correlated with proliferation [86]. Therefore, the effect of elastin peptides on the proliferation of salivary gland ductal cells was tested. The immortalized mouse submandibular ductal cell line (SIMS) cells were cultured on the various nanofiber scaffolds or glass, and the cells were counted at multiple time intervals: 4, 24, 48 and 72 hours. Figure 5 shows the total count of cells cultured on the different scaffolds at different time points. Cells cultured on elastin-containing scaffolds (EP-blend and EP-covalent) showed significantly less proliferation than cells cultured on PLGA nanofibers. This reduction in total cell count is attributed to reduction in cell proliferation rather than cell death, as the cell viability is high (≥ 90%) and not significantly different between the groups at all the time points (supplementary figure 1). Elastin incorporation reduced proliferation of mouse submandibular ductal cells, similar to keratinocytes [33].

3.6. Effect of elastin nanofiber modification on organization, morphology and clustering of SIMS cells

In order to assess the effect of elastin modification of the nanofiber scaffold on the cells' organization and morphology, SIMS cells were cultured on all the various scaffolds and their organization after 48 hours of seeding was assessed. Confocal microscopy images, Figure 6A, show that SIMS cells cultured on Elastin-PLGA fibers prepared by blend electrospinning (EP-blend) grew in closely-packed rounded cells showing obvious clustering and visibly smaller nuclear area indicative of minimal spreading with fewer stress actin fibers than cells grown on the other substrates.

To quantify cell clustering, the nearest neighbor distance between adjacent nuclei and the mean nuclear area of cell nuclei for subconfluent SIMS cells cultured on the different substrates were measured. The mean nearest neighbor distance is an established statistical indicator of spatial distribution of subjects [87]. The smaller the distance, the more closely-connected the cells are, which is epithelial-like and is necessary for the cells' barrier function and directional flow of saliva [7]. Figure 6B shows the mean nearest neighbor distance for SIMS cells cultured on the different substrates. As shown, elastin as a blend electrospinning modification (EP-blend) promoted significantly more close-packing of the cells, as indicated by the smallest nearest neighbor distance among the groups, Figure 6B. Interestingly, elastin as a covalent modification on the surface (EP-covalent) had the opposite effect. As shown in Figure 6B, covalent modification of PLGA nanofibers with elastin on the surface (EP-covalent) disrupted the close-packing of SIMS as indicated by a significant increase in the mean nearest neighbor distance as compared to PLGA fibers (P). The nuclear morphology is closely-associated with the cell cytoskeletal morphology; thus, the nuclear area can be used as an indicator of the cellular area and cell spreading [88]. Figure 6C shows that elastin as a blend electrospinning component (EP-blend) resulted in significantly smaller nuclear area, indicating less spreading. On the other hand, EP-covalent showed an increase in the mean nuclear area when compared to PLGA fibers (P). Interestingly, cells cultured on EP-blend nanofibers, showed significant increase in cell-scaffold integration, as cells were able to embed within the scaffold (55.8 ± 10.5 % of the cell height) as compared to 16.1± 4.6% and 18.3 ± 5.5% for EP-covalent and PLGA fibers, respectively, as shown in Figure 7C. Collectively, the cell organization, Figure 6A, the nearest neighbor distance measurements and the nuclear area measurements, Figures 6B and 6C, of SIMS cultured on the different scaffolds indicate that elastin as a blend electrospinning component of the fibrous body of the scaffold (EP-blend) and not as a surface modification of PLGA fibers (EP-covalent) is of benefit for epithelial cell organization, Figure 6, and cell-scaffold integration, Figure 7C. These data are consistent with the increased compliance of the EP-covalent scaffolds facilitating cell self-organization.

3.7. Effect of elastin nanofiber modification on SIMS cell apical polarization

Given that apicobasal polarity is a requirement for functioning ductal cells, we questioned if elastin in the PLGA nanofiber scaffolds could promote apical polarization of SIMS salivary epithelial cells. In order to test this hypothesis, SIMS cells were cultured on the different substrates and performed immunocytochemistry to detect tight junction proteins, occludin and ZO-1 [5–6], together with filamentous β-actin using immunocytochemistry and confocal imaging. Actin forms cytoskeletal filaments that are progressively concentrated at the apical membrane with polarization and that is also useful as an indicator of monolayer cell heights, which increase with cell apicobasal polarization [89].

Elastin, either as a blend electrospinning component (EP-blend) or as a covalently-conjugated motif (EP-covalent), promoted the apical localization of the three proteins, occludin, ZO-1, and F-actin. Figure 7A shows the XZ projections of the confocal microscopy Z-stacks taken for the cells grown on all the different substrates for 6 days, with the basal side of the cell in contact with the scaffold. Similar to our previous reports, [14], minimal ZO-1 polarization was detected for PLGA nanofibers without any noticeable apical

localization of actin and occludin, and all three proteins were laterally localized in cells grown on glass substrates. In agreement with this observation, a significant increase in the mean monolayer height of cells cultured on the elastin-containing scaffolds was observed with elastin as a blend electrospinning component showing the highest average monolayer height among the different substrates, as quantified in Figure 7B. Elastin, as a covalently conjugated surface molecule (EP-covalent), produced a slight increase in the average cell monolayer height as compared to PLGA. These data support the conclusion that elastin promotes apical polarization of submandibular duct epithelial cells through chemical signaling.

4. Discussion

Engineered scaffolds to promote salivary gland regeneration hold great promise for long-term treatment of salivary gland hypofunction. However, providing appropriate chemical, mechanical, and physical cues to direct salivary epithelial cell organization and function for regenerative medicine approaches has not yet been realized. Many current tissue engineering approaches use hydrogels, as they are compliant and permissive for cell self-organization, however, the closed structures formed do not readily provide an outlet for delivery of saliva to the mouth [90–94]. Therefore, a biocompatible scaffold that directs the growth of the salivary cells as an appropriately polarized monolayer is promising.

Since the low compliance, poor hydrophilicity and lack of biochemical cues associated with many biomaterials including nanofibers of synthetic polymers is not optimal for epithelial cell self-organization and function; however, in this study we investigated the utility of elastin to generate elastin-PLGA hybrid nanofibers that have more favorable elasticity, wettability and *in vivo*-like chemical structure. Elastin was introduced into our previously-developed PLGA nanofiber scaffolds [14, 23–24, 53] using two methods, blend electrospinning and covalent conjugation on the surface. Adding elastin to the PLGA scaffolds using either of the methods significantly improved its wettability, which is vital for cell-scaffold interactions [79–80]. This improvement in hydrophilicity is expected and can be attributed to the abundance of hydrophilic amine and carboxylic acid groups in elastin peptides. The increase in scaffold wettability was more significant for EP-covalent nanofibers, suggesting accumulation of more elastin on the surface as expected from the synthesis method (post-electrospinning covalent conjugation) [68].

Elastin, in its fibrous form, is known to confer mechanical elasticity and stretch-ability to the elastic fibers of the ECM, blood vessels and skin *in vivo* [31]. Here, it was demonstrated that blend electrospinning of elastin into the scaffold significantly improved the PLGA nanofiber scaffold elasticity, as shown by the reduction of the average Young's modulus from (4.29 MPa) for PLGA fibers (P) to (0.59 MPa) for elastin-PLGA nanofibers prepared by blend electrospinning (EP-blend). However, covalent conjugation of elastin on the surface of PLGA fibers post electrospinning (EP-covalent) increased the mean scaffold stiffness to (20.72 MPa) as compared to PLGA nanofibers (P), which was confirmed to be due to the chemical treatment of the fiber mat with EDC-mediated crosslinking. Physical characterization of the scaffolds confirmed that morphologically, elastin, as a blended component of the fiber mat (EP-blend), showed slightly more flattened fibers with more

bends and curves than PLGA nanofibers, which may be a visual indicator of the elasticity of the EP-blend scaffolds.

The cellular response to the scaffolds was evaluated in terms of proliferation, apical polarization and organization. Apical polarization, controlled proliferation, and cell height are intimately-related epithelial characteristics. As epithelial cell height increases, it is typically accompanied with cell differentiation and with a reduction in cell proliferation [86]. In this study, we noted that apicobasal polarity, and cell monolayer heights are promoted by elastin addition to the nanofibers using either blend electrospinning or covalent conjugation (EP-blend and EP-covalent). Cell proliferation was coordinately reduced as a result of elastin modification of the scaffolds. Since polarization and suppression of proliferation were observed for elastin-modified scaffolds whether the stiffer scaffold (EP-covalent, elastic modulus = 20.72 ± 5.978 MPa) or the softer scaffold (EP-blend, elastic modulus = 0.59 ± 0.356 MPa), while not observed for PLGA nanofibers (intermediate stiffness, elastic modulus = 4.29 ± 1.789 MPa), it is likely that that the biochemical nature of elastin peptides, rather than elastin's mechanical effect, is a major contributing factor for apicobasal polarization and suppression of proliferation. Also, modulation of cell proliferation by either suppression [33] or induction [62–64], in response to elastin peptides was reported elsewhere [33, 77–79]. However, a definitive conclusion on the causative factor of these cellular responses cannot be made as other possible factors could not be excluded in this study.

Self-organization and close cell-cell contact are characteristics of epithelial cells in tissues and are important for tissue structure and function [23]. In this respect, we found that EP-blend nanofibers promoted better epithelial organization than nanofibers with covalently conjugated elastin and the control substrates. These data imply that the elasticity of the scaffold, rather than its chemical structure, is causative in facilitating cell shape change and self-organization. In addition, the improved cellular infiltration into the blend elastin scaffold may also make the cells perceive the scaffold as a 3D environment which, in return, may support the observed cell self-organization.

5. Conclusions

Towards optimizing a scaffold for salivary gland regenerative medicine strategies, the potential of PLGA nanofiber modification with elastin, an ECM protein, using blend electrospinning and covalent conjugation, was investigated. This study demonstrated that the modification of PLGA nanofibers with elastin as a blend electrospinning component improved the overall characteristics of the nanofiber scaffolds which translated into desirable effects on salivary epithelial cells. Elastin incorporation by blend electrospinning improved the elasticity, wettability, and chemical nature of the nanofibers. This resulted in epithelial cell self-organization into clustered epithelial cells and less cell spreading. In addition, elastin promoted apical localization of occludin, ZO-1, and F-actin with an accompanying cell monolayer increase and proliferation decrease. The incorporation of elastin into PLGA nanofibers improved ability to culture salivary epithelial cells with more native epithelial characteristics without the requirement for chemical conjugation or micropatterning of the scaffold.

Elastin-PLGA nanofiber scaffolds have a strong potential applicability in salivary gland tissue regeneration and in regeneration of other epithelial organs. Collectively, our observations indicate that PLGA-elastin nanofiber scaffolds prepared by blend electrospinning (EP-blend) can provide appropriate chemical and/or mechanical signaling to direct the self-organization of differentiated epithelial cell monolayers. The EP-blend nanofiber scaffolds may be additionally useful for delivery of regeneration-stimulating factors and/or cells in regenerative medicine approaches for restoration of saliva production in patients with chronic salivary hypofunction.

Supplementary Material

Refer to Web version on PubMed Central for supplementary material.

Acknowledgments

This research was funded by the National Institutes of Health, National Institute of Dental and Craniofacial Research R01DE022467 to M.L and J.C., National Institutes of Health C06 RR015464 to the University at Albany, SUNY, National Science Foundation MRI award DBI0922830 to CNSE, and funds from the University at Albany, SUNY.

References

1. Eveson JW. Xerostomia. Periodontol 2000. 2008; 48:85–91. [PubMed: 18715359]
2. Kagami H, Wang S, Hai B. Restoring the function of salivary glands. Oral Dis. 2008; 14:15–24. [PubMed: 18173444]
3. Villa A, Connell C, Abati S. Diagnosis and management of xerostomia and hyposalivation. Ther Clin Risk Manag. 2015; 11:45–51. [PubMed: 25653532]
4. Tucker A. Salivary gland development. Semin Cell Dev Biol. 2007; 18:237–244. [PubMed: 17336109]
5. Shin K, Fogg VC, Margolis B. Tight Junctions and Cell Polarity. Annu Rev Cell Dev Biol. 2006; 22:207–235. [PubMed: 16771626]
6. Cereijido M, Contreras RG, Shoshani L, Flores-Benitez D, Larre I. Tight junction and polarity interaction in the transporting epithelial phenotype. Biochim Biophys Acta, Biomembr. 2008; 1778:770–793.
7. Baker OJ. Tight Junctions in Salivary Epithelium. J Biomed Biotechnol. 2010; 2010:1–13.
8. Epstein FH, Fish EM, Molitoris BA. Alterations in Epithelial Polarity and the Pathogenesis of Disease States. N Engl J Med. 1994; 330:1580–1588. [PubMed: 8177249]
9. Reichmann E. Oncogenes and epithelial cell transformation. Semin Cancer Biol. 1994; 5:157–165. [PubMed: 8061331]
10. Bissell MJ, Radisky D. Putting tumours in context. Nat Rev Cancer. 2001; 1:46–54. [PubMed: 11900251]
11. Frantz C, Stewart KM, Weaver VM. The extracellular matrix at a glance. J Cell Sci. 2010; 123:4195–4200. [PubMed: 21123617]
12. Muiznieks LD, Keeley FW. Molecular assembly and mechanical properties of the extracellular matrix: A fibrous protein perspective. Biochim Biophys Acta, Mol Basis Dis. 2013; 1832:866–875.
13. Daley WP, Kohn JM, Larsen M. A focal adhesion protein-based mechanochemical checkpoint regulates cleft progression during branching morphogenesis. Dev Dyn. 2011; 240:2069–2083. [PubMed: 22016182]
14. Cantara SI, Soscia DA, Sequeira SJ, Jean-Gilles RP, Castracane J, Larsen M. Selective functionalization of nanofiber scaffolds to regulate salivary gland epithelial cell proliferation and polarity. Biomaterials. 2012; 33:8372–8382. [PubMed: 22938763]

15. Nam K, Jones JP, Lei P, Andreadis ST, Baker OJ. Laminin-111 peptides conjugated to fibrin hydrogels promote formation of lumen containing parotid gland cell clusters. Biomacromolecules. 2016; 17:2293–2301. [PubMed: 27151393]
16. Pradhan S, Zhang C, Jia X, Carson DD, Witt R, Farach-Carson MC. Perlecan domain IV peptide stimulates salivary gland cell assembly in vitro. Tissue Eng Part A. 2009; 15:3309–3320. [PubMed: 19382872]
17. Pradhan S, Liu C, Zhang C, Jia X, Farach-Carson MC, Witt RL. Lumen formation in three-dimensional cultures of salivary acinar cells. Otolaryngol Head Neck Surg. 2010; 142:191–195. [PubMed: 20115973]
18. Aframian DJ, Cukierman E, Nikolovski J, Mooney DJ, Yamada KM, Baum BJ. The Growth and Morphological Behavior of Salivary Epithelial Cells on Matrix Protein-Coated Biodegradable Substrata. Tissue Eng. 2000; 6:209–216. [PubMed: 10941215]
19. Handorf AM, Zhou Y, Halanski MA, Li WJ. Tissue stiffness dictates development, homeostasis, and disease progression. Organogenesis. 2015; 11:1–15. [PubMed: 25915734]
20. Mosier A, Peters S, Larsen M, Cady N. Microfluidic platform for the elastic characterization of mouse submandibular glands by atomic force microscopy. Biosensors. 2014; 4:18–27. [PubMed: 25587408]
21. Peters SB, Naim N, Nelson DA, Mosier AP, Cady NC, Larsen M. Biocompatible tissue scaffold compliance promotes salivary gland morphogenesis and differentiation. Tissue Eng Part A. 2014; 20:1632–1642. [PubMed: 24410370]
22. Peters SB, Nelson DA, Kwon HR, Koslow M, Desantis KA, Larsen M. TGFβ signaling promotes matrix assembly during mechanosensitive embryonic salivary gland restoration. Matrix Biol. 2015; 43:109–124. [PubMed: 25652203]
23. Sequeira SJ, Soscia DA, Oztan B, Mosier AP, Jean-Gilles R, Gadre A, Cady NC, Yener B, Castracane J, Larsena M. The regulation of focal adhesion complex formation and salivary gland epithelial cell organization by nanofibrous PLGA scaffolds. Biomaterials. 2012; 33:3175–3186. [PubMed: 22285464]
24. Soscia DA, Sequeira SJ, Schramm RA, Jayarathanam K, Cantara SI, Larsen M, Castracane J. Salivary gland cell differentiation and organization on micropatterned PLGA nanofiber craters. Biomaterials. 2013; 34:6773–6784. [PubMed: 23777914]
25. Nivison-Smith, L., Weiss, A. Elastin based constructs. In: Eberli, D., editor. Regenerative Medicine and Tissue Engineering - Cells and Biomaterials, InTech. 2011. p. 323-340.
26. Karnik SK. A critical role for elastin signaling in vascular morphogenesis and disease. Development. 2003; 130:411–423. [PubMed: 12466207]
27. Mariani TJ, Sandefur S, Pierce RA. Elastin in Lung Development. Exp Lung Res. 1997; 23:131–145. [PubMed: 9088923]
28. Wise SG, Yeo GC, Hiob MA, Rnjak-Kovacina J, Kaplan DL, Ng MK, Weiss AS. Tropoelastin: A versatile, bioactive assembly module. Acta Biomater. 2014; 10:1532–1541. [PubMed: 23938199]
29. Starcher B, Aycock RL, Hill CH. Multiple Roles for Elastic Fibers in the Skin. J Histochem Cytochem. 2005; 53:431–443. [PubMed: 15805418]
30. Almine JF, Bax DV, Mithieux SM, Nivison-Smith L, Rnjak J, Waterhouse A, Wise SG, Weiss AS. Elastin-based materials. Chem Soc Rev. 2010; 39:3371. [PubMed: 20449520]
31. Anwar RA. Elastin: A brief Review. Biochem Educ. 1990; 18:162–166.
32. Rodgers UR, Weiss AS. Cellular interactions with elastin. Pathol Biol. 2005; 53:390–398. [PubMed: 16085115]
33. Fujimoto N, Tajima S, Ishibashi A. Elastin peptides induce migration and terminal differentiation of cultured keratinocytes via 67 kDa elastin receptor in vitro: 67 kDa elastin receptor is expressed in the keratinocytes eliminating elastic materials in elastosis perforans serpiginosa. J Invest Dermatol. 2000; 115:633–639. [PubMed: 10998135]
34. Jin E, Lee PT, Jeon WB, Li WJ. Effects of elastin-like peptide on regulation of human mesenchymal stem cell behavior. Regen Eng Transl Med. 2016; 2:85–97.
35. Lorber M. Elastic fibers in the duct system of the rat submandibular salivary gland. Anat Rec. 1992; 234:335–347. [PubMed: 1443662]

36. Black JB. The structure of the salivary glands of the human soft palate. J Morphol. 1977; 153:107–117. [PubMed: 894716]
37. Wollina U. One-stage reconstruction of soft tissue defects with the sandwich technique: Collagen-elastin dermal template and skin grafts. J Cutan Aesthet Surg. 2011; 4:176. [PubMed: 22279382]
38. Boekema BKHL, Vlig M, Damink LO, Middelkoop E, Eummelen L, Bühren AV, Ulrich MM. Effect of pore size and cross-linking of a novel collagen-elastin dermal substitute on wound healing. J Mater Sci Mater Med. 2013; 25:423–433. [PubMed: 24178984]
39. Lamme EN, Vries HJD, Veen HV, Gabbiani G, Westerhof W, Middelkoop E. Extracellular matrix characterization during healing of full-thickness wounds treated with a collagen/elastin dermal substitute shows improved skin regeneration in pigs. J Histochem Cytochem. 1996; 44:1311–1322. [PubMed: 8918906]
40. Janorkar AV, Rajagopalan P, Yarmush ML, Megeed Z. The use of elastin-like polypeptide–polyelectrolyte complexes to control hepatocyte morphology and function in vitro. Biomaterials. 2008; 29:625–632. [PubMed: 18006054]
41. Chuang TH, Stabler C, Simionescu A, Simionescu DT. Polyphenol-stabilized tubular elastin scaffolds for tissue engineered vascular grafts. Tissue Eng Part A. 2009; 15:2837–2851. [PubMed: 19254115]
42. Wise SG, Byrom MJ, Waterhouse A, Bannon PG, Ng MK, Weiss AS. A multilayered synthetic human elastin/polycaprolactone hybrid vascular graft with tailored mechanical properties. Acta Biomater. 2011; 7:295–303. [PubMed: 20656079]
43. Wong CS, Liu X, Xu Z, Lin T, Wang X. Elastin and collagen enhances electrospun aligned polyurethane as scaffolds for vascular graft. J Mater Sci Mater Med. 2013; 24:1865–1874. [PubMed: 23625321]
44. Han J, Lazarovici P, Pomerantz C, Chen X, Wei Y, Lelkes PI. Co-electrospun blends of PLGA, gelatin, and elastin as potential nonthrombogenic scaffolds for vascular tissue engineering. Biomacromolecules. 2011; 12:399–408. [PubMed: 21182235]
45. Koens MJW, Krasznai AG, Hanssen AEJ, Hendriks T, Praster R, Daamen WF, van der Vliet JA, van Kuppevelt TH. Vascular replacement using a layered elastin-collagen vascular graft in a porcine model: one week patency versus one month occlusion. Organogenesis. 2015; 11:105–121. [PubMed: 26060888]
46. Sell SA, Mcclure MJ, Barnes CP, Knapp DC, Walpoth BH, Simpson DG, Bowlin GL. Electrospun polydioxanone–elastin blends: potential for bioresorbable vascular grafts. Biomed Mater. 2006; 1:72–80. [PubMed: 18460759]
47. Wise S, Byrom M, Bannon P, Weiss A, Ng M. Electrospun Elastin-based Vascular Grafts. Heart Lung Circ. 2008; 17:S19.
48. Gao J, Crapo P, Nerem R, Wang Y. Co-expression of elastin and collagen leads to highly compliant engineered blood vessels. J Biomed Mater Res A. 2008; 85A:1120–1128.
49. Kumar VA, Caves JM, Haller CA, Dai E, Liu L, Grainger S, Chaikof EL. Acellular vascular grafts generated from collagen and elastin analogs. Acta Biomater. 2013; 9:8067–8074. [PubMed: 23743129]
50. Mcclure MJ, Sell SA, Simpson DG, Walpoth BH, Bowlin GL. A three-layered electrospun matrix to mimic native arterial architecture using polycaprolactone, elastin, and collagen: A preliminary study. Acta Biomater. 2010; 6:2422–2433. [PubMed: 20060934]
51. Ravi S, Caves JM, Martinez AW, Haller CA, Chaikof EL. Incorporation of fibronectin to enhance cytocompatibility in multilayer elastin-like protein scaffolds for tissue engineering. J Biomed Mater Res A. 2012; 101A:1915–1925.
52. Li M, Mondrinos MJ, Chen X, Gandhi MR, Ko FK, Lelkes PI. Co-electrospun poly(lactide-co-glycolide), gelatin, and elastin blends for tissue engineering scaffolds. J Biomed Mater Res A. 2006; 79A:963–973.
53. Jean-Gilles R, Soscia D, Sequeira S, Melfi M, Gadre A, Castracane J, Larsen M. Novel modeling approach to generate a polymeric nanofiber scaffold for salivary gland cells. J Nanotechnol Eng Med. 2010; 1:031008–031016.
54. Hartman O, Zhang C, Adams EL, Farach-Carson MC, Petrelli NJ, Chase BD, Rabolt JF. Biofunctionalization of electrospun PCL-based scaffolds with perlecan domain IV peptide to

create a 3-D pharmacokinetic cancer model. Biomaterials. 2010; 31:5700–5718. [PubMed: 20417554]

55. Laoide BM, Courty Y, Gastinne I, Thibaut C, Kellermann O, Rougeon F. Immortalised mouse submandibular epithelial cell lines retain polarised structural and functional properties. J Cell Sci. 1996; 109:2780–2789.
56. Eidet JR, Pasovic L, Maria R, Jackson CJ, Utheim TP. Objective assessment of changes in nuclear morphology and cell distribution following induction of apoptosis. Diagn Pathol. 2014; 9:92. [PubMed: 24885713]
57. Giesbers M, Marcelis ATM, Zuilhof H. Simulation of XPS C1s Spectra of Organic Monolayers by Quantum Chemical Methods. Langmuir. 2013; 29:4782–4788. [PubMed: 23548381]
58. López GP, Castner DG, Ratner BD. XPS O 1s binding energies for polymers containing hydroxyl, ether, ketone and ester groups. Surf Interface Anal. 1991; 17:267–272.
59. Taucher TC, Hehn I, Hofmann OT, Zharnikov M, Zojer E. Understanding Chemical versus Electrostatic Shifts in X-ray Photoelectron Spectra of Organic Self-Assembled Monolayers. J Phys Chem C. 2016; 120:3428–3437.
60. Ariza MCADJCBA, Rodríguez-Castellón E, Rico R, Benavente J, Muñoz M, Oleinikova M. X-Ray Photoelectron Spectroscopy Analysis of Di-(2-ethylhexyl) Phosphoric Acid Activated Membranes. J Colloid Interface Sci. 2000; 226:151–158. [PubMed: 11401359]
61. Wang Y, Li P, Kong L. Chitosan-Modified PLGA Nanoparticles with Versatile Surface for Improved Drug Delivery. AAPS PharmSciTech. 2013; 14(2):585–592. [PubMed: 23463262]
62. Araujo J, Padrão J, Silva JP, Dourado F, Correia DM, Botelho G, Gomez Ribelles L, Lanceros-Méndez S, Sencadas V. Processing and characterization of α-elastin electrospun membranes. Appl Phys A. 2013; 115:1291–1298.
63. Popescu MC, Vasile C, Craciunescu O. Structural analysis of some soluble elastins by means of FT-IR and 2D IR correlation spectroscopy. Biopolymers. 2010; 93:1072–1084. [PubMed: 20665685]
64. Erbetta CD. Synthesis and characterization of Poly(D,L-Lactide-co-Glycolide) copolymer. J Biomater Nanobiotechnol. 2012; 03:208–225.
65. Wang C, Li Y, Ding G, Xie X, Jiang M. Preparation and characterization of graphene oxide/poly(vinyl alcohol) composite nanofibers via electrospinning. J Appl Polym Sci. 2012; 127:3026–3032.
66. Hang Y, Zhang Y, Jin Y, Shao H, Hu X. Preparation and characterization of electrospun silk fibroin/sericin blend fibers. J Mater Res. 2011; 26:2931–2937.
67. Smith GP, Mclaughlin AW, Clarkson AN, Gordon KC, Walker GF. Raman microscopic imaging of electrospun fibers made from a polycaprolactone and polyethylene oxide blend. Vib Spectrosc. 2017; 92:27–34.
68. Yoo HS, Kim TG, Park TG. Surface-functionalized electrospun nanofibers for tissue engineering and drug delivery. Adv Drug Deliv Rev. 2009; 61:1033–1042. [PubMed: 19643152]
69. Agarwal S, Wendorff JH, Greiner A. Use of electrospinning technique for biomedical applications. Polymer. 2008; 49:5603–5621.
70. Han J, Lazarovici P, Pomerantz C, Chen X, Wei Y, Lelkes PI. Co-Electrospun Blends of PLGA, Gelatin, and Elastin as Potential Nonthrombogenic Scaffolds for Vascular Tissue Engineering. Biomacromolecules. 2011; 12:399–408. [PubMed: 21182235]
71. Suchý TCACA, Šupová M, Sauerová P, Verdánová M, Sucharda Z, Rýglová Š, Žaloudková M, Sedláček R, Kalbáčová MH. The effects of different cross-linking conditions on collagen-based nanocomposite scaffolds—an in vitro evaluation using mesenchymal stem cells. Biomed Mater. 2015; 10:065008. [PubMed: 26586611]
72. Haugh MG, Murphy CM, Mckiernan RC, Altenbuchner C, O'brien FJ. Crosslinking and Mechanical Properties Significantly Influence Cell Attachment, Proliferation, and Migration Within Collagen Glycosaminoglycan Scaffolds. Tissue Eng Part A. 2011; 17:1201–1208. [PubMed: 21155630]
73. Baker SR, Banerjee S, Bonin K, Guthold M. Determining the mechanical properties of electrospun poly-ε-caprolactone (PCL) nanofibers using AFM and a novel fiber anchoring technique. Mater Sci Eng C Mater Biol Appl. 2016; 59:203–212. [PubMed: 26652365]

74. Madurantakam PA, Rodriguez IA, Garg K, Mccool JM, Moon PC, Bowlin GL. Compression of Multilayered Composite Electrospun Scaffolds: A Novel Strategy to Rapidly Enhance Mechanical Properties and Three Dimensionality of Bone Scaffolds. Adv Mater Sci Eng. 2013; 2013:1–9.
75. Gosline J, Lillie M, Carrington E, Guerette P, Ortlepp C, Savage K. Elastic Proteins: Biological Roles and Mechanical Properties, Elastomeric Proteins. Philos Trans R Soc Lond B Biol Sci. 2002; 357:121–132. [PubMed: 11911769]
76. Muiznieks LD, Keeley FW. Molecular assembly and mechanical properties of the extracellular matrix: A fibrous protein perspective. Biochim biophys acta, Mol basis dis. 2013; 1832:866–875.
77. Araujo J, Padrão J, Silva JP, Dourado F, Correia DM, Botelho G, et al. Processing and characterization of α-elastin electrospun membranes. Appl Phys A. 2013; 115:1291–1298.
78. Mason, BN., Califano, JP., Reinhart-King, CA. Matrix stiffness: a regulator of cellular behavior and tissue formation. In: Bhatia, KS., editor. Engineering Biomaterials for Regenerative Medicine. Springer; 2011. p. 19-37.
79. Xu L, Siedlecki CA. Effects of surface wettability and contact time on protein adhesion to biomaterial surfaces. Biomaterials. 2007; 28:3273–3283. [PubMed: 17466368]
80. Goddard J, Hotchkiss J. Polymer surface modification for the attachment of bioactive compounds. Prog Polym Sci. 2007; 32:698–725.
81. Jordan SW, Haller CA, Sallach RE, Apkarian RP, Hanson SR, Chaikof EL. The effect of a recombinant elastin-mimetic coating of an ePTFE prosthesis on acute thrombogenicity in a baboon arteriovenous shunt. Biomaterials. 2007; 28:1191–1197. [PubMed: 17087991]
82. Çelebi BCBC, Cloutier M, Balloni R, Mantovani D, Bandiera A. Human Elastin-Based Recombinant Biopolymers Improve Mesenchymal Stem Cell Differentiation. Macromol Biosci. 2012; 12:1546–1554. [PubMed: 23042756]
83. Ito S, Ishimaru S, Wilson SE. Effect of coacervated -elastin on proliferation of vascular smooth muscle and endothelial cells. Angiology. 1998; 49:289–297. [PubMed: 9555932]
84. Kamoun A, Landeau JM, Godeau G, Wallach J, Duchesnay A, Pellat B, Hornebeck W. Growth stimulation of human skin fibroblasts by elastin-derived peptides. Cell Adhesion Comm. 1995; 3:273–281.
85. Tajima S, Wachi H, Uemura Y, Okamoto K. Modulation by elastin peptide VGVAPG of cell proliferation and elastin expression in human skin fibroblasts. Arch Dermatol Res. 1997; 289:489–492. [PubMed: 9266029]
86. Bilder D. Epithelial polarity and proliferation control: links from the Drosophila neoplastic tumor suppressors. Genes Dev. 2004; 18:1909–1925. [PubMed: 15314019]
87. Clark PJ, Evans FC. Distance to nearest neighbor as a measure of spatial relationships in populations. Ecology. 1954; 35:445–453.
88. Friedl P, Wolf K, Lammerding J. Nuclear mechanics during cell migration. Curr Opin Cell Biol. 2011; 23:55–64. [PubMed: 21109415]
89. Asnacios A, Hamant O. The mechanics behind cell polarity. Trends Cell Biol. 2012; 22:584–591. [PubMed: 22980034]
90. Baker OJ, Schulz DJ, Camden JM, Liao Z, Peterson TS, Seye CI, Petris MJ, Weisman GA. rat parotid gland cell differentiation in three-dimensional culture. Tissue Eng Part C Methods. 2010; 16:1135–1144. [PubMed: 20121592]
91. Wei C, Larsen M, Hoffman MP, Yamada KM. Self-organization and branching morphogenesis of primary salivary epithelial cells. Tissue Eng. 2007; 13:721–735. [PubMed: 17341161]
92. Shubin AD, Felong TJ, Graunke D, Ovitt CE, Benoit DS. Development of Poly(Ethylene Glycol) hydrogels for salivary gland tissue engineering applications. Tissue Eng Part A. 2015; 21:1733–1751. [PubMed: 25762214]
93. Liyanage W, Vats K, Rajbhandary A, Benoit DSW, Nilsson BL. Multicomponent dipeptide hydrogels as extracellular matrix-mimetic scaffolds for cell culture applications. Chem Commun. 2015; 51:11260–11263.
94. Kleinman HK, Martin GR. Matrigel: Basement membrane matrix with biological activity. Semin Cancer Biol. 2005; 15:378–386. [PubMed: 15975825]

Statement of significance

Regenerating the salivary glands by mimicking the extracellular matrix (ECM) is a promising approach for long term treatment of salivary gland damage. Despite their topographic similarity to the ECM, electrospun fibers of synthetic polymers lack the biochemical complexity, elasticity and hydrophilicity of the ECM. Elastin is an ECM protein abundant in the salivary glands and responsible for tissue elasticity. Although it's widely used for tissue regeneration of other organs, little is known about its utility in regenerating the salivary tissue. This study describes the use of elastin to improve the elasticity, hydrophilicity and biochemical complexity of synthetic nanofibers and its potential in directing in vivo-like organization of epithelial salivary cells which helps the design of efficient salivary gland regeneration scaffolds.

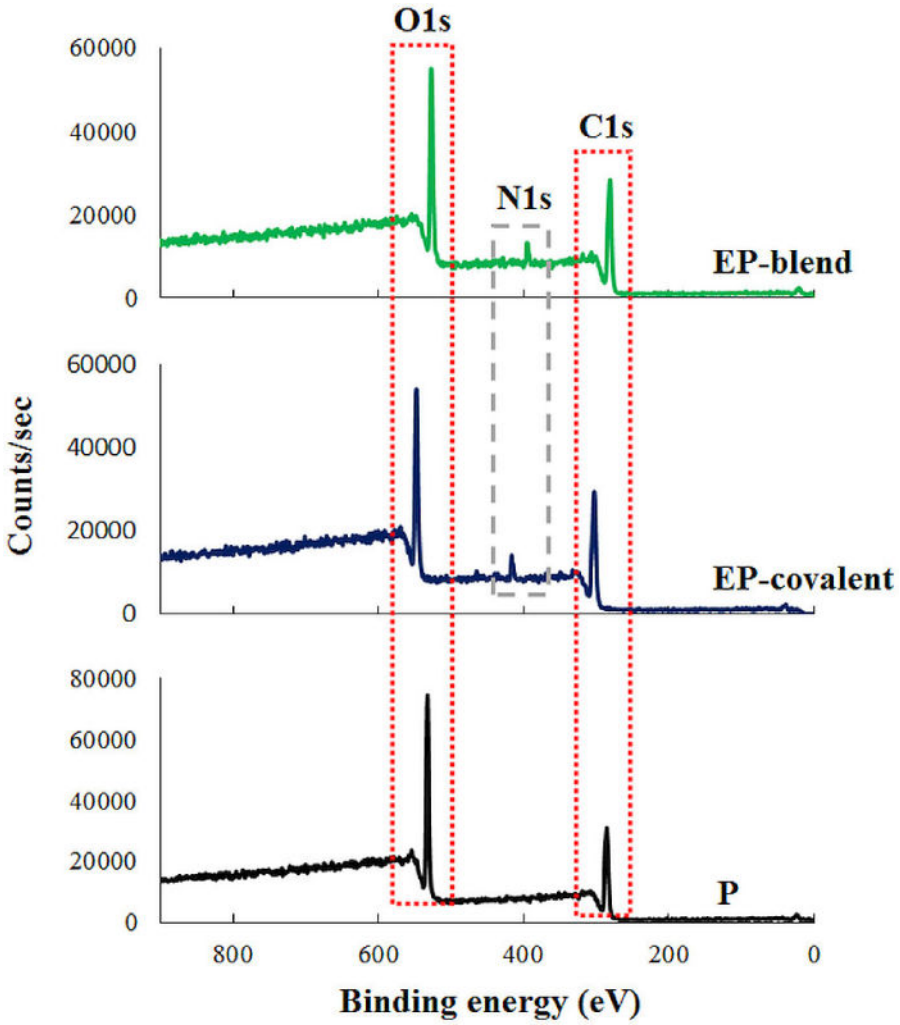

Figure 1.

Confirmation of elastin inclusion in the nanofiber scaffolds using the XPS spectra of the nanofiber scaffolds. The appearance of the N1s peak around 400 eV in EP-blend and EP-covalent nanofibers and its absence in PLGA indicates the presence of elastin. EP-blend, elastin-PLGA-blend nanofibers; EP-covalent, elastin-PLGA-covalent nanofibers; P, PLGA nanofibers.

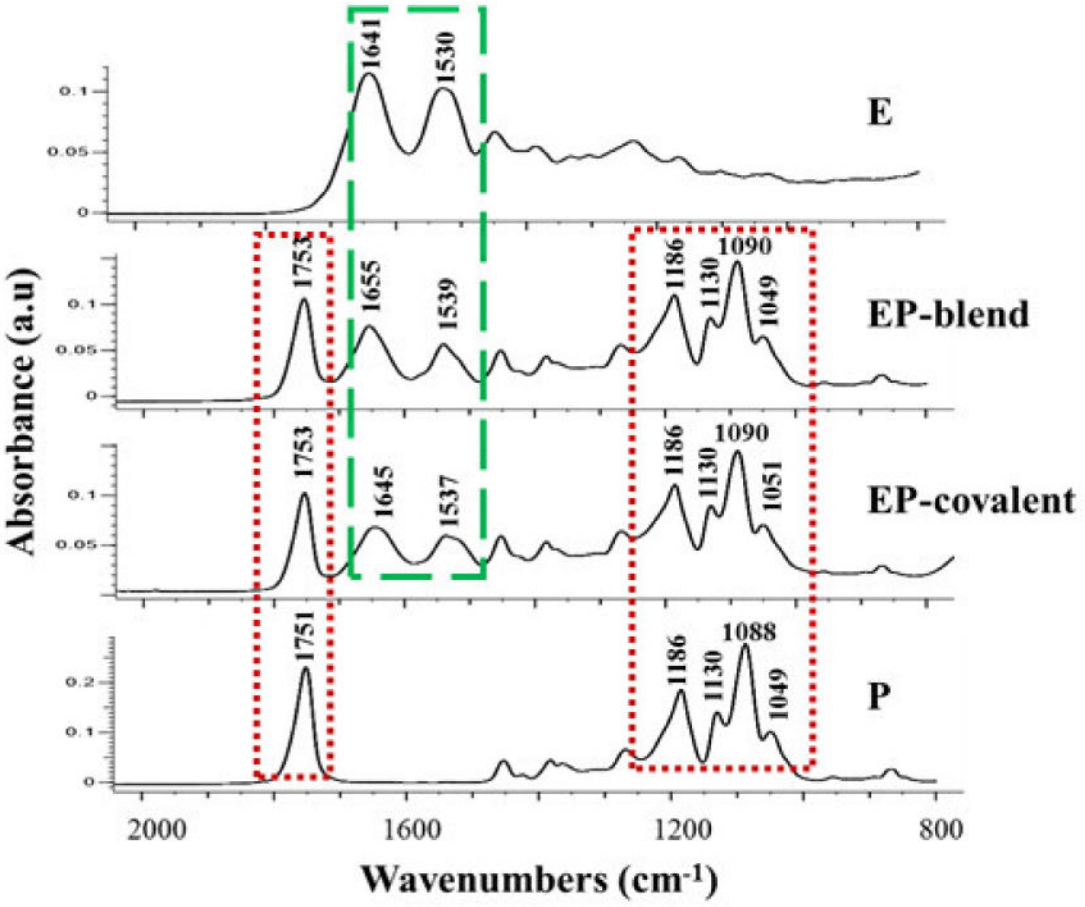

Figure 2.

FTIR characterization of the nanofiber scaffolds. The appearance of peaks between 1530 and 1660 cm^{-1} corresponding to N-C=O stretching vibrations of primary and secondary amide bonds in elastin confirms the presence of elastin in the nanofiber scaffolds and indicates the preservation of elastin peptides after inclusion into the nanofibers. E, elastin powder; EP-blend, elastin-PLGA-blend nanofibers; EP-covalent, elastin-PLGA-covalent nanofibers; P, PLGA nanofibers.

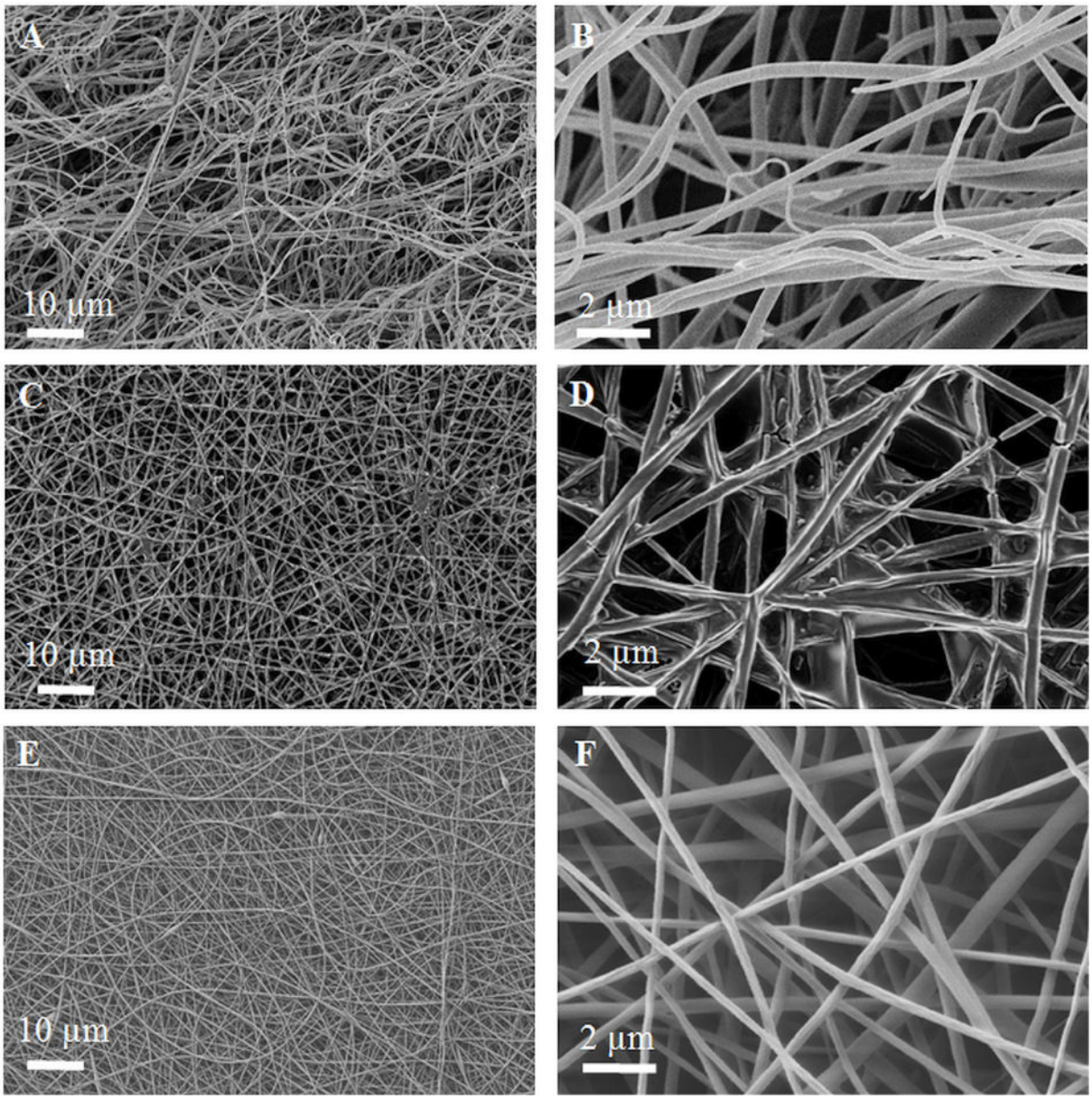

Figure 3.

SEM characterization of the nanofiber scaffolds. A, B- EP-blend, C, D- EP-covalent and E, F- P nanofibers. Unlike PLGA nanofibers, EP-blend nanofibers include curved fibers.

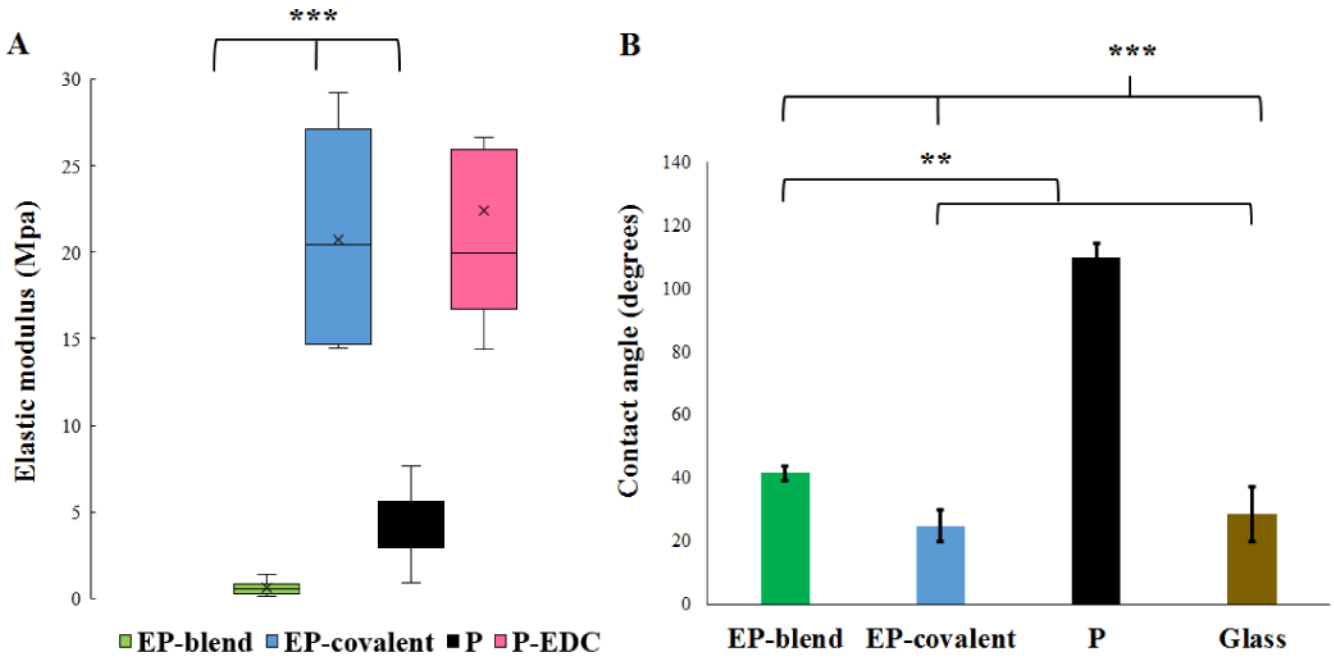

Figure 4.

Elastin improves the mechanical compliance and hydrophilicity of the nanofiber scaffolds. A- AFM mechanical characterization of the nanofiber scaffolds. Elastin functionalization by blend electrospinning conferred elasticity to the nanofiber scaffolds. EP-blend nanofibers show the smallest Young's modulus at 0.59 ± 0.356 MPa as compared to 20.72 ± 5.978 MPa for EP-covalent, 4.29 ± 1.789 MPa for P and 20.4 ± 8.6 MPa for P-EDC. EP-blend, EP-covalent and P are significantly different from each other, while P-EDC and EP-covalent are not significantly different. B- Elastin functionalization and inclusion in the electrospun fibers by either blend electrospinning (EP-blend) or covalent conjugation (EP-covalent) significantly increases the wettability of the nanofiber scaffolds as indicated by the decrease in contact angle measurements. Contact angle measurement results are presented as mean ± SD; 42 ± 2.36°, 25 ± 5.25°, 110 ± 4.56°, 25.25 ± 4.1° for EP-blend, EP-covalent, P and glass, respectively. ANOVA with Bonferroni's post-test; *$p < 0.05$, **$p < 0.01$, ***$p < 0.001$. P-EDC, PLGA fibers treated with EDC chemistry only without adding elastin.

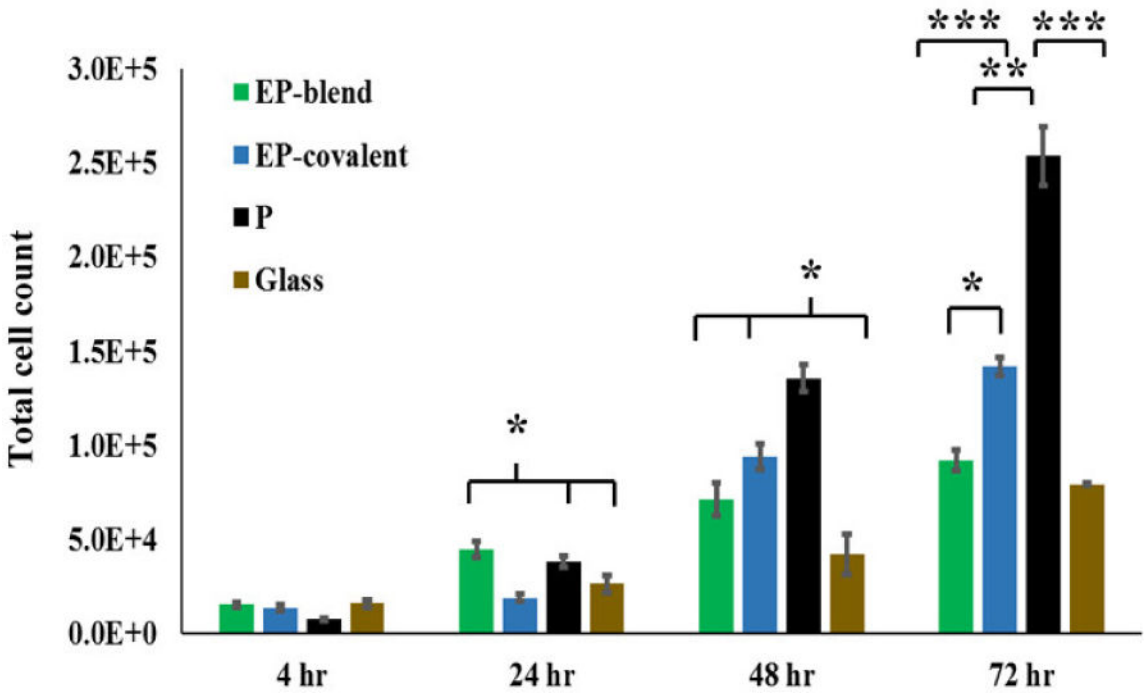

Figure 5.

Effect of elastin inclusion in nanofibers on SIMS cell proliferation. SIMS cells were seeded on the scaffolds indicated and allowed to grow for up to 72 hours. Viable cells were counted every 24 hours. After 24 hrs, cells grown on elastin-containing nanofibers generally show reduced cell numbers as compared to cells grown on PLGA nanofibers. Total cell number graphs indicate that reduction in proliferation appeared as early as 24 hours for EP-covalent and at 48 hours for EP-blend. This effect was more prominent for EP-blend, especially at 72 hours. Results shown are presented as mean ± SEM. Single-factor ANOVA with Bonferroni's post-test. *$p < 0.05$, **$p < 0.01$, ***$p < 0.001$.

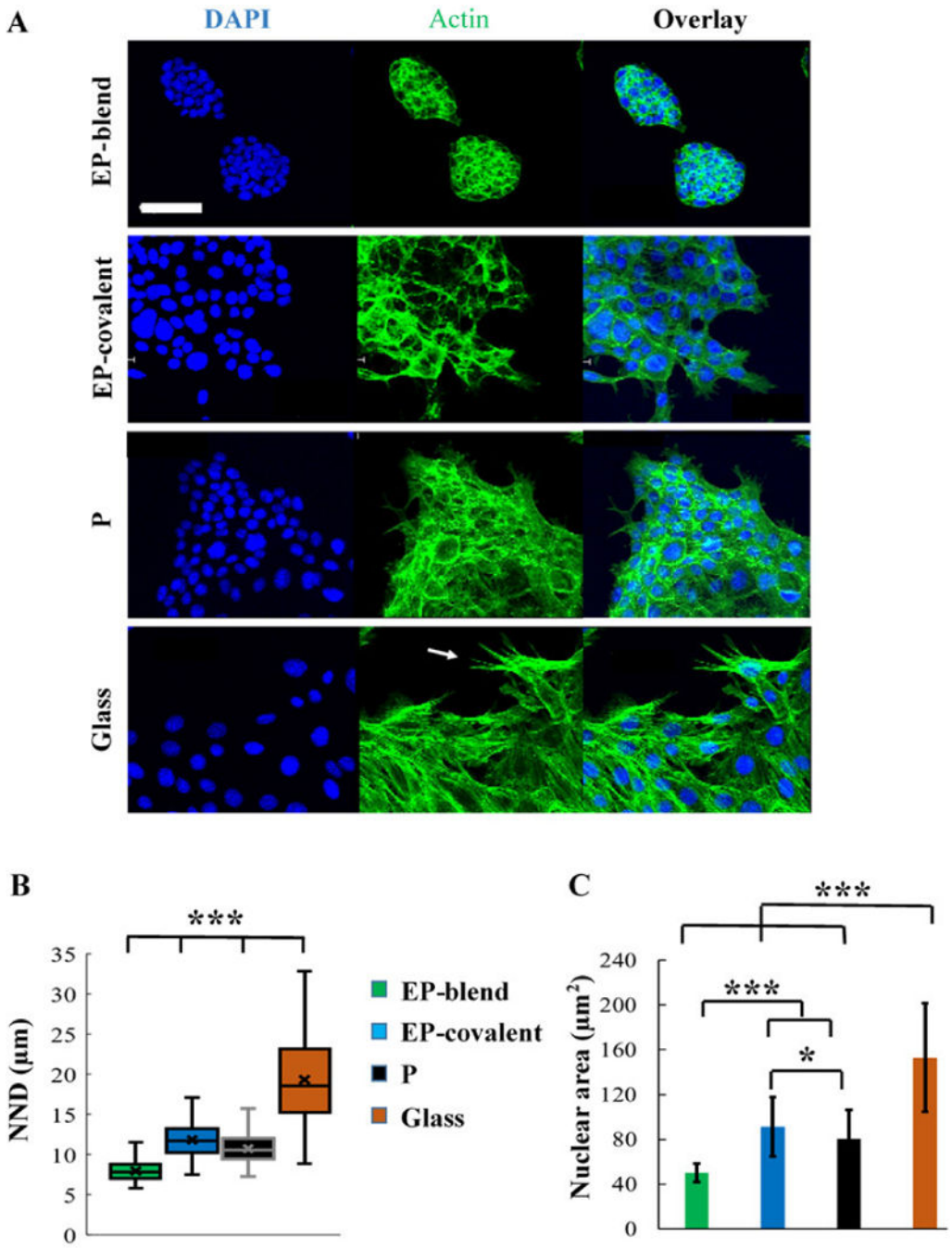

Figure 6.

Elastin as blend electrospinning component supports epithelial cell clustering organization. A- Representative XY confocal images of SIMS cells grown on the different scaffolds for 48 hours showing the clustered cell appearance of SIMS grown on EP-blend as compared to the other scaffolds. Stress fibers are most prominent for SIMS grown on glass (arrow) and least prominent for EP-blend. DAPI (blue), nuclei; F-Actin, green. Scale bar, 50 μm. B- Quantification of cell clustering using nearest neighbor distance (NND) measurements. EP-blend shows the smallest distance, meaning the most clustering. C- Quantification of cell

spreading using average nuclear area measurements. EP-blend shows the smallest nuclear area indicating most clustering. Mean ± SD. Single factor ANOVA with Bonferroni's post-test; *$p < 0.05$, *** $p < 0.001$.

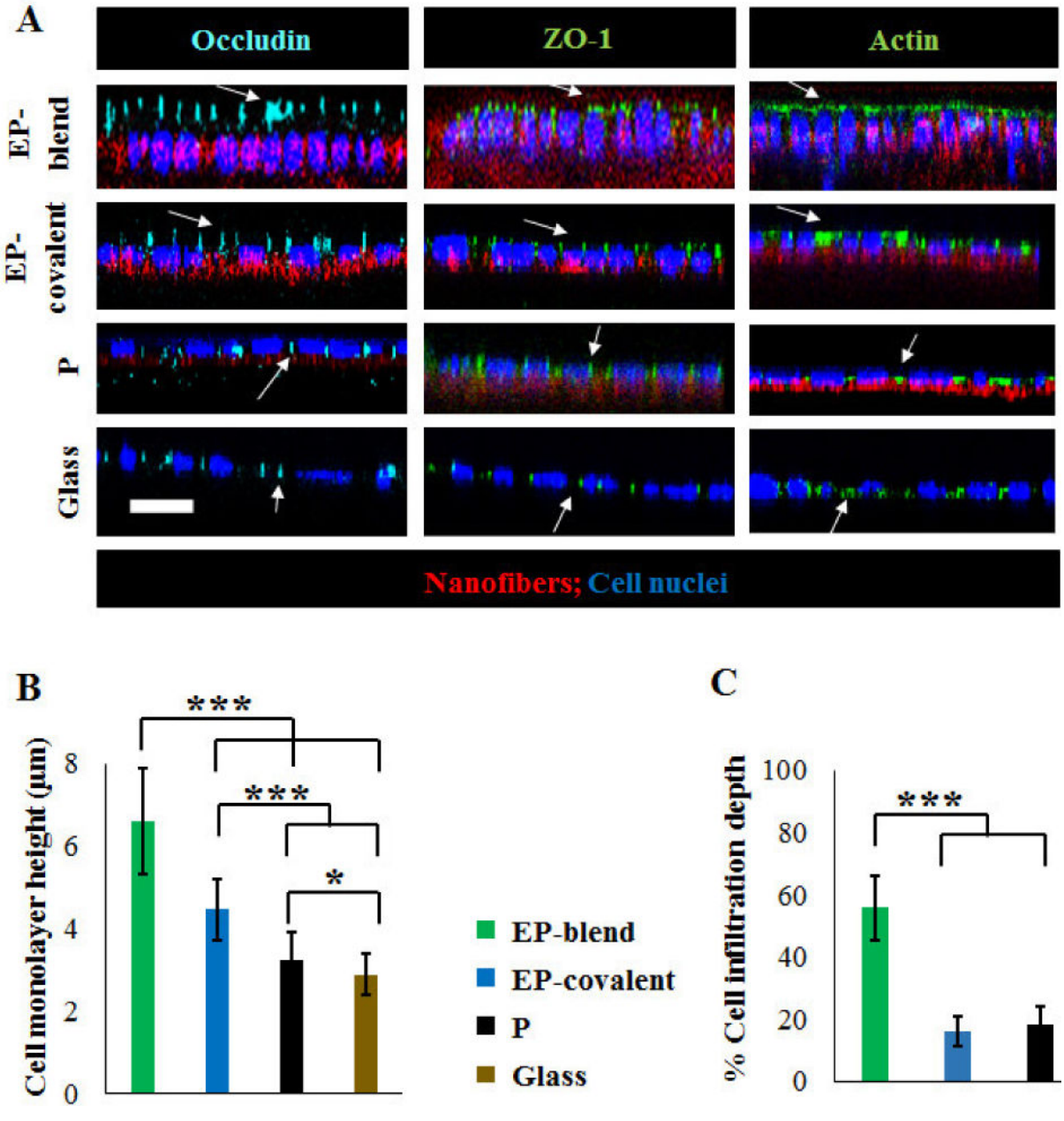

Figure 7.

Apicobasal epithelial cell polarization in response to elastin. Tight junction proteins and actin localization in SIMS cells cultured on different substrates, 6-days post-seeding. A- Representative XZ confocal projections show that elastin-modified nanofibers (EP-blend and EP-covalent) show the most apical (above the nucleus) polarization of occludin, ZO-1, and actin. Scale bar, 10 μm. Occludin (cyan); ZO-1 (green, second column); Actin (green, third column); DAPI (blue), nuclei; nanofibers (red). B- Average monolayer height of SIMS grown on the different substrates. Cells grown on elastin-modified scaffolds show significantly higher average monolayer heights than cells grown on PLGA nanofibers or glass. This is very noticeable for EP-blend nanofibers. Mean ±SD. C- Integration of SIMS

cells within the nanofiber scaffolds characterized by % cell infiltration depth. The infiltration depth is defined as the cell height embedded within the nanofiber scaffold divided by the total cell height. EP-blend nanofibers promote increased cell infiltration. Mean ± SD. ANOVA with Bonferroni's post-test; *$p < 0.05$, ***$p < 0.001$.